# The Canary Intermediate Poleward Undercurrent: Not Another Poleward Undercurrent in an Eastern Boundary Upwelling System

P. VÉLEZ-BELCHÍ,[a] V. CAÍNZOS,[b] E. ROMERO,[b] M. CASANOVA-MASJOAN,[b] C. ARUMÍ-PLANAS,[b] D. SANTANA-TOSCANO,[b] A. GONZÁLEZ-SANTANA,[a] M. D. PÉREZ-HERNÁNDEZ,[b] AND A. HERNÁNDEZ-GUERRA[b]

[a] *Centro Oceanográfico de Canarias, Instituto Español de Oceanografía, Santa Cruz de Tenerife, Canary Islands, Spain*
[b] *Unidad Océano y Clima, Instituto de Oceanografía y Cambio Global, Universidad de Las Palmas de Gran Canaria, Unidad Asociada ULPGC-CSIC, Canary Islands, Spain*

(Manuscript received 16 June 2020, in final form 2 June 2021)

ABSTRACT: Poleward undercurrents are well-known features in eastern boundary upwelling systems. In the California Current upwelling system, the California poleward undercurrent has been widely studied, and it has been demonstrated that it transports nutrients from the equatorial waters to the northern limit of the subtropical gyre. However, in the Canary Current upwelling system, the Canary intermediate poleward undercurrent (CiPU) has not been properly characterized, despite recent studies arguing that the dynamics of the eastern Atlantic Ocean play an important role in the Atlantic meridional overturning circulation, specifically on its seasonal cycle. Here, we use trajectories of Argo floats and model simulations to characterize the CiPU, including its seasonal variability and its driving mechanism. The Argo observations show that the CiPU flows from 26°N, near Cape Bojador, to approximately 45°N, near Cape Finisterre and flows deeper than any poleward undercurrent in other eastern boundaries, with a core at a mean depth of around 1000 dbar. Model simulations manifest that the CiPU is driven by the meridional alongshore pressure gradient due to general ocean circulation and, contrary to what is observed in the other eastern boundaries, is still present at 1000 dbar as a result of the pressure gradient between the Antarctic Intermediate Waters in the south and Mediterranean Outflow waters in the north. The high seasonal variability of the CiPU, with its maximum strength in autumn and minimum in spring, is due to the poleward extension of AAIW, forced by Ekman pumping in the tropics.

KEYWORDS: Continental shelf/slope; North Atlantic Ocean; Boundary currents; Meridional overturning circulation; Ocean circulation; Upwelling/downwelling

## 1. Introduction

Poleward undercurrents are well-known features in eastern boundary upwelling systems (EBUS) (Neshyba et al. 1989). In the California Current eastern boundary upwelling system (CalCEBUS), the California Undercurrent (CU) is the subsurface poleward flow and has been widely described using hydrographic observations (Huyer et al. 1989; Huyer 1989), Lagrangian floats (Collins et al. 1996, 2000, 2003, 2004, 2018; Garfield et al. 1999), and gliders (Todd et al. 2011), supported by model simulations (Connolly et al. 2014). The importance of the CU in maintaining the high productivity of the CalCEBUS has also been demonstrated (Thomson and Krassovski 2010). In the other EBUS, undercurrents have also been reported, although they have not been as extensively studied as the CalCEBUS. In the Humboldt Current eastern boundary upwelling system (HumCEBUS), the poleward-flowing undercurrent is the Peru–Chile Undercurrent (PCU) and is characterized by a high-salinity and low-oxygen core at 150–200 m, although it is noticeable from the surface down to 300 m depth. The PCU has been observed between 18° and 48°S, with maximum velocities between 23° and 33°S. The PCU has been observed all year round, although with the largest transport during summer. The importance of the PCU in supplying cold, high-salinity and low-oxygen waters to the upper ocean in the northern coast of Chile has been demonstrated (Fonseca 1989; Hill et al. 1998). In the Benguela Current eastern boundary upwelling system (BenCEBUS) there is a deep poleward current, below 2000 m, that transports North Atlantic Deep Water from the deep western boundary current across the Atlantic (Kersalé et al. 2019; Baker-Yeboah et al. 2010), although this current has only been observed close to the slope, and south of 33°S. In the upper layers, there are only a few observations indicating a poleward flow that is shallower than 500 m and over the inner shelf (Shillington et al. 2006; Hill 1998; Nelson 1989).

In the Canary Current eastern boundary upwelling system (CanCEBUS), early studies in the 1980s (Haynes and Barton 1990) using SST, drifters, Sea Soar data, and moorings found evidence of a strong poleward flow over the Iberian continental shelf and slope during September 1986, although the authors concluded that satellite data indicated a similar situation in other years. This poleward flow, known as the Iberia Poleward Current, is associated with the salty tongue of Mediterranean outflow waters (MOW) in the upper 600 m (Haynes and Barton 1990). Short-term current-meter observations corroborated that the poleward flow occurred along the continental

Casanova-Masjoan: Deceased.

*Corresponding author*: P. Vélez-Belchí, pedro.velez@ieo.es

DOI: 10.1175/JPO-D-20-0130.1

slope, reaching depths deeper than 600 m, consistent with previous observations along the Portuguese coast (Fiuza 1982; Meincke et al. 1975; Teles-Machado et al. 2016). Some authors (Zenk and Armi 1990) linked the spreading of Mediterranean waters to the cores of the undercurrent that flows poleward off Portugal, while other authors (Haynes and Barton 1990; McCreary et al. 1986) attributed this poleward flow to the meridional thermohaline forcing. Some model simulations also stated that the meridional alongshore pressure gradient (APG) plays a predominant role on the forcing of this poleward flow (Peliz et al. 2003, 2005). More recently, Teles-Machado et al. (2016) stated that the main forcing of the Iberian Poleward Current, that occupies the top 350 m, is the so-called Joint Effect of Baroclinicity and Relief (JEBAR), although they recognized that its role decreases substantially in the months of stronger poleward flow.

Off the northwest coast of Africa, early studies in the 1970s and 1980s (Mittelstaedt et al. 1975; Mittelstaedt 1976, 1983, 1989), using the signature of the Antarctic Intermediate Waters (AAIW) and the South Atlantic Central Waters in sparse hydrographic observations, and a few weeks of current-meter records, hypothesized a slope poleward current from the tropical North Atlantic. This slope current flows at depths between 100 and 200 m off Senegal and Mauritania, deepening while on its way poleward, reaching 1000-m depth north of the Canary Islands.

Since these early studies, the regional knowledge of the poleward flow in the Canary Current eastern boundary upwelling system has increased mainly in the vicinity of the Canary Islands. At the latitude of the Canary Islands, specifically at the Lanzarote passage, between Africa and the Canary Islands, a poleward flow has been widely described and confirmed using hydrographic observations (Hernández-Guerra et al. 2003, 2001), satellite observations (Pérez-Hernández et al. 2015) and long-term moorings (Fraile-Nuez et al. 2010; Pérez-Hernández et al. 2015). Several authors (Hernández- Guerra et al. 2001, 2003; Fraile-Nuez et al. 2010; Pérez-Hernández et al. 2015; Vélez-Belchí et al. 2017; Casanova-Masjoan et al. 2020) have described a high seasonal cycle for this poleward flow and have attributed it to the different forcing between the flow through the Lanzarote Passage and the Canary Current, and therefore to the different dynamics driving the flow in the open ocean and on the African slope (Casanova-Masjoan et al. 2020; Vélez-Belchí et al. 2017; Pérez-Hernández et al. 2015). However, the mechanism driving the poleward flow in the Lanzarote Passage is still controversial. Machín and Pelegrí (2009) and Machín et al. (2010) attributed the poleward flow during autumn to an isopycnal stretching due to wind forcing, while Pérez-Hernández et al. (2015) associated it to the recirculation of the Canary Current around the Canary Islands Archipelago. In the surface waters of the Lanzarote Passage, some authors (Pelegrí et al. 2005; Laiz et al. 2012) have associated the poleward flow to the upwelling off northwest Africa and the Canary Upwelling Current. Farther south, between Cape Verde and the Canary Islands, and during November 2008, the poleward flow was described by Peña-Izquierdo et al. (2012) as a 50-km-wide jet, with its core at around 300 m but reaching the surface, and with an estimated transport of 2.8 Sv ($1\,\mathrm{Sv} \equiv 10^6\,\mathrm{m^3\,s^{-1}}$) at 18°N and 1.7 Sv at 24°N. Modeling studies between Cape Ghir and the Iberian Peninsula (Batteen et al. 2000, 2007; Mason et al. 2011) showed a poleward undercurrent at approximately 1000–1400-m depth, and within 50 km of the shelf break. On a basinwide scale, Hagen (2001) recently reviewed the hypotheses and observations in the CanCEBUS and attributed the poleward flow to the meridional APG off the continental slope. For these authors, this alongshore pressure gradient is forced by wind and buoyancy and is modulated by the variations on the zonal slope of the continental shelf. Hagen (2001) described different, and disconnected, poleward undercurrents for each upwelling region of the CanCEBUS, one for the Iberian Peninsula and one off northwest Africa. A poleward flow along the tropical eastern boundary, at depths of 950–1150 m, was described using neutrally buoyant SOFAR floats (Fratantoni and Richardson 1999).

Despite the abovementioned regional studies, from an observational point of view, there is still no evidence showing a continuity of the poleward flow from the region northwest of Africa to the Atlantic coast of the Iberian Peninsula. Except in the Lanzarote Passage, most of the observations are limited to a few weeks, and to geostrophic and waters masses analysis, with its associated uncertainty (Laiz et al. 2012; Pérez-Hernández et al. 2013). The location of the core of the poleward flow is still unclear (Barton 1989) since most of the observations are in different years and months. Moreover, the few and sparse observations of the poleward flow prevent from establishing a driving mechanism for the undercurrent (Hill et al. 1998; Neshyba et al. 1989).

It is important to understand the variability and driving mechanism of the poleward undercurrent of the CanCEBUS for two reasons. The first one is to understand its role in feeding the upwelled waters, as is the case for the CalCEBUS. The second reason is to understand the role of the eastern boundary of the North Atlantic in the Atlantic meridional overturning circulation (AMOC). Recent studies (Chidichimo et al. 2010; Kanzow et al. 2010) using data from the U.K.–U.S. Rapid Climate Change–Meridional Overturning Circulation and Heatflux Array, known as RAPID-MOCHA, attributed most of the peak-to-peak seasonal cycle of the AMOC to the eastern boundary of the Atlantic. Using a linear Rossby wave model, these studies concluded that the seasonal variation of the upper- to midocean transport is almost entirely due to changes in stratification at the eastern boundary, which is caused by local wind stress curl variations, or to the flow concentrated within a narrow band along the eastern boundary (Pérez-Hernández et al. 2015; Kanzow et al. 2010). However, Vélez-Belchí et al. (2017) demonstrated that Rossby waves cannot explain the seasonal cycle of the AMOC and that the seasonal cycle of the eastern boundary of the Atlantic at 26.5°N is due, for the central and surface waters, to the recirculation of the Canary Current and, at intermediate levels, to the seasonal cycle of the poleward undercurrent.

In general, the CanCEBUS and the CalCEBUS are similar and comparable, and usually knowledge gaps about the poleward undercurrent in the CanCEBUS are filled with the experience in the CalCEBUS. However, there are some differences

TABLE 1. Argo data used in the four EBUS during the period from July 2013 to July 2018 for the analyses. The floats with at least four Argo cycles (~40 days) of poleward trajectories (fourth column) were used in Fig. 1. In parentheses in the third column is the percentage of total days of poleward trajectories from the total days of Argo observations in the corresponding EBUS. In parentheses in the fourth column is the percentage of floats, from the total in the corresponding EBUS, that had poleward trajectories. The uncertainty in the last column is the standard error of the mean.

| | Total No. of Argo floats | Total No. of Argo profiles | Total days of poleward trajectories | Floats with poleward trajectories | Mean days in poleward trajectories |
|---|---|---|---|---|---|
| CalCEBUS | 175 | 19 786 | 636 (0.3%) | 8 (4.6%) | 79.5 ± 12.4 |
| CanCEBUS | 273 | 20 441 | 5960 (2.9%) | 53 (19.4%) | 112.4 ± 12.0 |
| HumCEBUS | 220 | 18 243 | 500 (0.3%) | 9 (4.1%) | 55.5 ± 11.2 |
| BenCEBUS | 201 | 12 161 | 630 (0.9%) | 7 (3.5%) | 90.0 ± 33.9 |

between the poleward undercurrents of the CalCEBUS and the CanCEBUS that suggest different forcing mechanisms, and therefore different variability. The most striking difference is that the observed core of the poleward flow in the CanCEBUS, the Canary Intermediate Poleward Undercurrent (CiPU), is deeper (~1000 dbar) than the core of the CU (~300 dbar). The scarce observations in the HumCEBUS and the BenCEBUS also suggest that the CiPU is unique within the four comparable EBUS, in the sense that the other poleward flows are shallower.

Here, taking advantage of the quasi-Lagrangian behavior of the Argo floats (Argo 2019) during its drift at the parking depth, we report on the continuity of the poleward undercurrent from 25°N, near Cape Bojador, to approximately 45°N, near Cape Finisterre, in the northwest coast of Spain. Using simulations, validated with long-term mooring observations, we examine the seasonal variability of the poleward undercurrent and demonstrate that the APG, contrary to what happens in the CalCEBUS, is still observed below 500 dbar and drives the CiPU. This APG is due to general ocean circulation and, contrary to what is observed in the other eastern boundaries, is still present at 1000 dbar because of the differences between the two intermediate water masses found in the CanCEBUS, the AAIW and the MOW.

## 2. Data and methods

### a. Argo trajectories

The YoMaHa database of Argo velocities at the parking depth (Lebedev et al. 2007), updated until March 2018, was used to identify the Argo floats used in this study. We selected the along-slope drift segments of subsurface trajectories in all the CEBUS for the floats with parking depth at 1000 dbar, that drifted along-slope longer than four Argo dives (~40 days). We have chosen 40 days to maximize the number of observations but to avoid selecting poleward along-slope drift segments that are due to mesoscale activity.

Once the Argo floats were identified, the full set of measurements for each float, including the measured pressure at the parking depth, were used to verify the actual trajectory of the float. From a total of 273 floats in the CanCEBUS region, bounded by 25°–5°W and 20°–45°N, 53 floats describe a poleward flow (Table 1). To avoid selecting Argo floats with spurious trajectories due to drift at the surface or the ascent/descent to the parking depth, we did a comparison with the ANDRO database (Ollitrault and Colin de Verdière 2013). Although the ANDRO database has a processing algorithm that overcomes problems associated with drift at the surface or the ascent/descent of the Argo float, the data are only available until October 2017. In the time period when the YoMaHa and the ANDRO database are coincident, none of the Argo floats selected with a poleward component in the YoMaHa database describes different behavior in the ANDRO database.

### b. Argo climatology

We used the global mean of temperature and salinity from the Argo derived climatology (Roemmich and Gilson 2009) at a 1/6° resolution, with data from 1998 to 2017.

### c. Mooring data

From 1999 to 2007, a mooring, known as Eastern Boundary Current-4 (EBC4) (Hernández-Guerra et al. 2003; Fraile-Nuez et al. 2010; Pérez-Hernández et al. 2015), was maintained in the Lanzarote Passage at 28.2°N, 13.5°W, at a depth of 1280 dbar (Fig. 1b). The mooring had five current meters at approximately 150, 300, 520, 870, and 1230 dbar, which record velocity, temperature, salinity, and pressure. The shallower three current meters were located in the upper layers, occupied by North Atlantic Central Waters; the lower two current meters are in intermediate layers containing AAIW and MOW, respectively. The sampling time interval for the instruments is 2 h. In this paper, to obtain the mean circulation, we use data collected between January 1998 and December 2007 for the 870-dbar current meter. During these nine years the mooring has been recovered and deployed 11 times for maintenance. As described by Fraile-Nuez et al. (2010), the mooring velocities used were rotated to the principal angle; and this angle was obtained by minimizing the sum of the squares of the normal distance. With the magnitude of the rotated velocity, the monthly climatology was computed (Fig. 2) from the nine years of daily data as described by Fraile-Nuez et al. (2010).

### d. Model simulations

Hindcast model simulations from the Ocean General Circulation Model for the Earth Simulator (OFES) were used in the area enclosed by 20°–5°W and 20°–45°N. The simulations were done by JAMSTEC, based on MOM3, in a global domain with a horizontal resolution of 1/10° and 54 vertical levels, computed

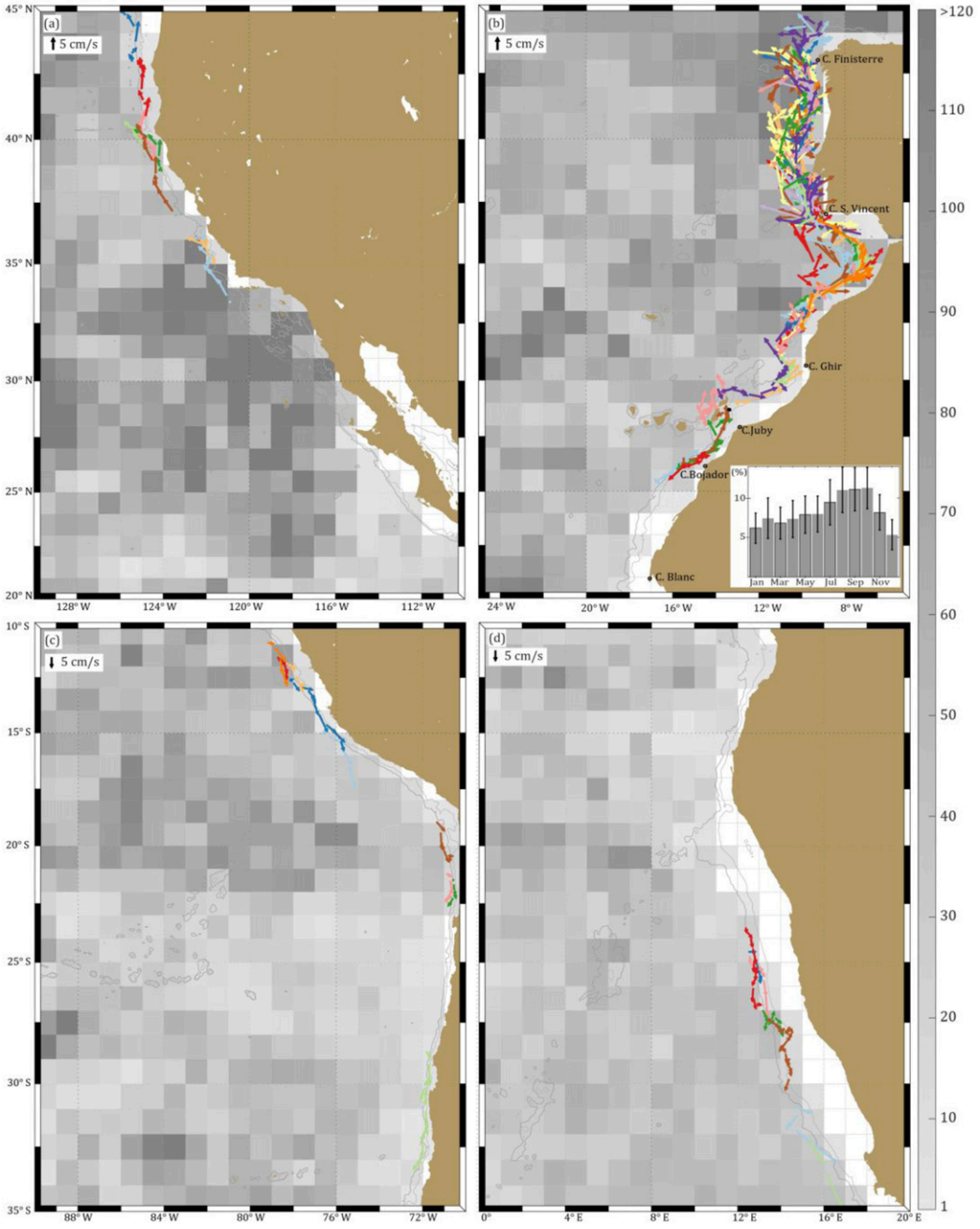


FIG. 1. Trajectory of the CiPU from Argo floats. Selected Argo poleward trajectories at the (a) California Current, (b) Canary Current, (c) Humboldt Current, and (d) Benguela Current eastern boundary upwelling systems. Only floats with parking depth at 1000 dbar that drifted poleward for, at least, four Argo cycles (~40 days) were considered. The number of floats with poleward trajectories in the figures is given in the fourth column of Table 1. Each one of the floats is represented with a different color. The background field represents the total number of Argo profiles, binned in a 1° × 1° grid. Only bin cells without Argo profiles appear as white and are bounded by light-gray lines. For reference, the 1000- and 2000-m isobaths are presented as a gray line and dark-gray line, respectively. Dark-gray circles in (b) show the main topographic and geographical features referred to in the text, and the black circle between Cape Juby and Lanzarote marks the mooring in the Lanzarote passage. The inset in (b) is the monthly percentage of Argo profiles of the selected poleward trajectories with respect to the total number of Argo profiles within 3° west of the coast, with uncertainties computed using bootstrap.

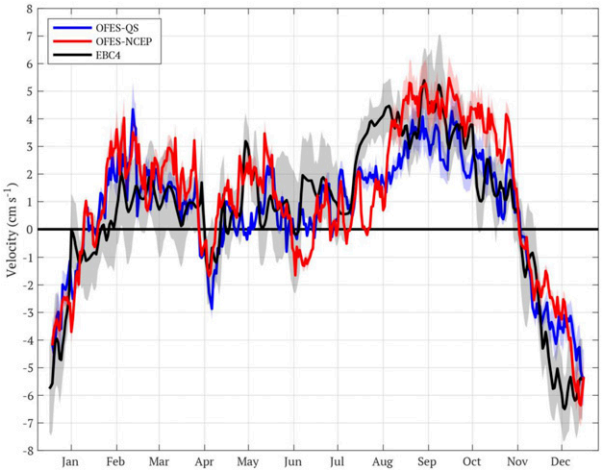


FIG. 2. Validation of the Ocean General Circulation Model of the Earth Simulator (Masumoto et al. 2004) in the CanCEBUS. The black line is the average monthly climatology of the current meter at 870 dbar from the long-term mooring located in the Lanzarote Passage as computed by Fraile-Nuez et al. (2010) and Hernández-Guerra et al. (2003). The blue and red lines correspond to average monthly climatology of the velocity OFES simulations forced with QuikSCAT and NCEP–NCAR reanalysis winds, respectively, at the same location and depth of the mooring data. For both, current-meter and model data, the velocities were rotated to the principal axis of the mooring observations at 870 dbar (51.2° clockwise) and can be considered to be along-slope velocities, positive poleward. The standard error of the mean is represented as the shaded area around each line.

each 3 days (Masumoto et al. 2004). Two different wind forcing were used in the simulations, a daily mean QuickSCAT (QS) wind stress, and a daily mean of NCEP–NCAR reanalysis data. Both the simulations forced by QS and NCEP–NCAR reanalysis winds covered a common period of time between January 1998 and December 2005. Monthly means and 3-day data, including temperature, salinity, surface height and velocity, were provided by the Asia-Pacific Data Research Center, which is a part of the International Pacific Research Center at the University of Hawai'i at Mānoa, funded in part by the National Oceanic and Atmospheric Administration (NOAA).

The validation of both simulations of the OFES model was done with velocity observations from the 870-dbar current meter of the EBC4 mooring (Fig. 2). The average monthly climatology of the mooring velocity rotated along its principal angle was compared with the average monthly climatology obtained by both OFES simulations at the same location and depth that was also rotated to the same principal angle (51.2° clockwise). Relative dynamic height was computed from salinity, temperature and pressure from OFES simulations referenced to the surface. The dynamic height (DH) was computed taking the surface as reference level and incorporating the sea surface height of the OFES model. The DH anomaly was computed subtracting the alongshore averaged vertical profile. The standard error of the mean is used as uncertainty in all the computed quantities.

## 3. Results

### a. *Along-slope Argo trajectories*

Taking advantage of the quasi-Lagrangian behavior of the Argo floats during their drift at the parking depth, we observe that the CanCEBUS is the EBUS with the largest number of poleward trajectories and total days of poleward trajectories (Fig. 1 and Table 1). In the CanCEBUS, taking into account only Argo trajectories with parking depth at 1000 dbar, 53 floats drifted poleward longer than 40 days (i.e., four Argo dives; Table 1). In the CanCEBUS, the Argo floats trajectories show an overall continuous along-slope poleward flow from south of Cape Bojador (26°N) to the northwest coast of Spain, north of Cape Finisterre (44°N) (Fig. 1b). South of 25°N, there are only a few Argo observations (Fig. 1b) and none of them had a poleward trajectory longer than four Argo dives. These 53 floats, which represent 19.4% of the Argo floats in the area, spent, on average, 112.4 ± 12.0 days drifting poleward, with a total of 5960 days of poleward drifting, which represents 2.9% of the total days of Argo observations in the area (Table 1).

In contrast, in the other EBUS, with similar Argo coverage, only a few Argo floats described poleward trajectories. In the CalCEBUS, only eight Argo-float trajectories, which represents 4.6% of the total 175 floats in the whole area, described a poleward trajectory. On average, each one spent 79.5 ± 12.4 days drifting poleward, recording a total of 636 days of poleward trajectories, 0.3% of the total days of Argo observations in the area (Table 1 and Fig. 1a). In the HumCEBUS, only nine Argo floats, 4.1% of the total of 220 in the area, drifted poleward (Fig. 1c). These nine Argo floats were concentrated in two areas, south of 16°S and around 20°S. The total days of registered poleward trajectories, 500, represented only 4.1% of the total days of Argo observations in the area. In the BenCEBUS, seven Argo floats, 3.5% of the total 201 floats in the area, described poleward trajectories. The total days of registered poleward trajectories were 630, representing only 0.9% of the total days of Argo observations in the area. The percentage of Argo floats with poleward trajectories in the CanCEBUS is 4.2 times as large as in the CalCEBUS, the second EBUS in the percentage of Argo floats with poleward trajectories. The percentage of days of poleward trajectories in the CanCEBUS is 3.2 times as large as in the BenCEBUS, the second EBUS in the percentage of days of poleward trajectories. These observations, in similar areas and with a similar total number of Argo floats, indicate that the mean core of the poleward currents in the CalCEBUS, HumCEBUS, and BenCEBUS is at a different depth than the CiPU in the CanCEBUS.

The mean velocity estimated for the CiPU at the CanCEBUS, using the Argo trajectories at the parking depth, is ~4.9 ± 0.1 cm s$^{-1}$. Four selected Argo floats show continuous trajectories from the Canary Islands to Cape Ghir, from Cape Ghir to Cape Saint Vincent and from Cape Saint Vincent to Cape Finisterre (Fig. 3). This is also different from the other EBUS, where the continuity of the poleward flow is not observed. The high number of total days of poleward trajectories in the CanCEBUS permits us to determine its monthly distribution. The CiPU presents some seasonality, with more

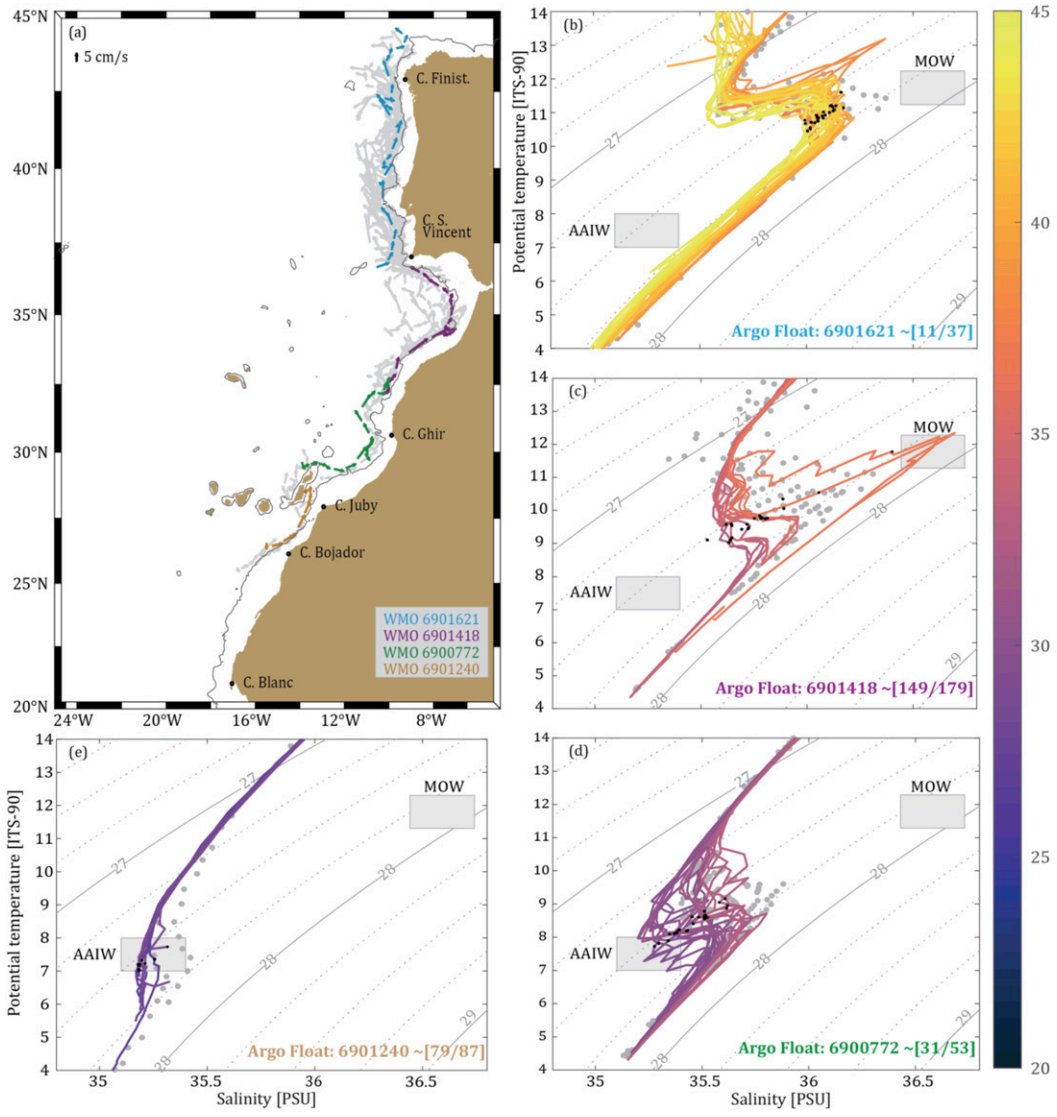


FIG. 3. Water masses along the trajectory of the CiPU at the CanCEBUS. (a) Selected Argo trajectories along the CiPU, with gray arrows showing all of the poleward trajectories, and a black arrow in the upper-left corner as scale. The black line corresponds to the 1000-m isobath. (b)–(e) The $\theta$–$S$ diagram of the profiles sampled by each one of the Argo floats in (a), from north [in (b)] to south [in (e)]. All $\theta$–$S$ diagrams have the same salinity and potential temperature range, with a color scale indicating latitude; the gray lines (solid and dashed) denote the $\sigma_\theta$ (kg m$^{-3}$) isolines; the gray dots represent the mean climatology from *World Ocean Atlas 2005* (Locarnini et al. 2006; Antonov et al. 2006); and the black dots are the Argo observations at 1000 m (parking depth of Argo floats) measured during the drifting period of the float. Gray rectangles indicate the characteristic properties of the purest AAIW and MOW in the CanCEBUS.

data from July to October, and less data during the winter months (Fig. 1b).

The analysis of the water masses at the parking depth of the Argo floats in the CanCEBUS (Fig. 3) indicates that the CiPU is not associated with any particular water mass. The southernmost float, between Cape Bojador (25°N) and Cape Juby, sampled AAIW, that are characterized by minimum values of salinity, as low as 35.17 at 6.8°C (~27.50 kg m$^{-3}$) (Fig. 3e). Between Cape Juby and north of Cape Ghir, the hydrographic observations from float 6900772 show an increase in the lower salinity of the AAIW and an increase in the relative maximum of salinity at ~27.75 kg m$^{-3}$ due to the mixture with the MOW (Fig. 3d). North of Cape Ghir and to Cape San Vincente, the AAIW signal disappears while there is an increase in the salinity values, consequence of the presence of purer MOW, that reach values up to 36.7 at 12.35°C (~27.75 kg m$^{-3}$) (Fig. 3c). The northernmost float (6901261) reaches values up to 36.31 at 13.19°C (~27.50 kg m$^{-3}$) and shows the characteristics of

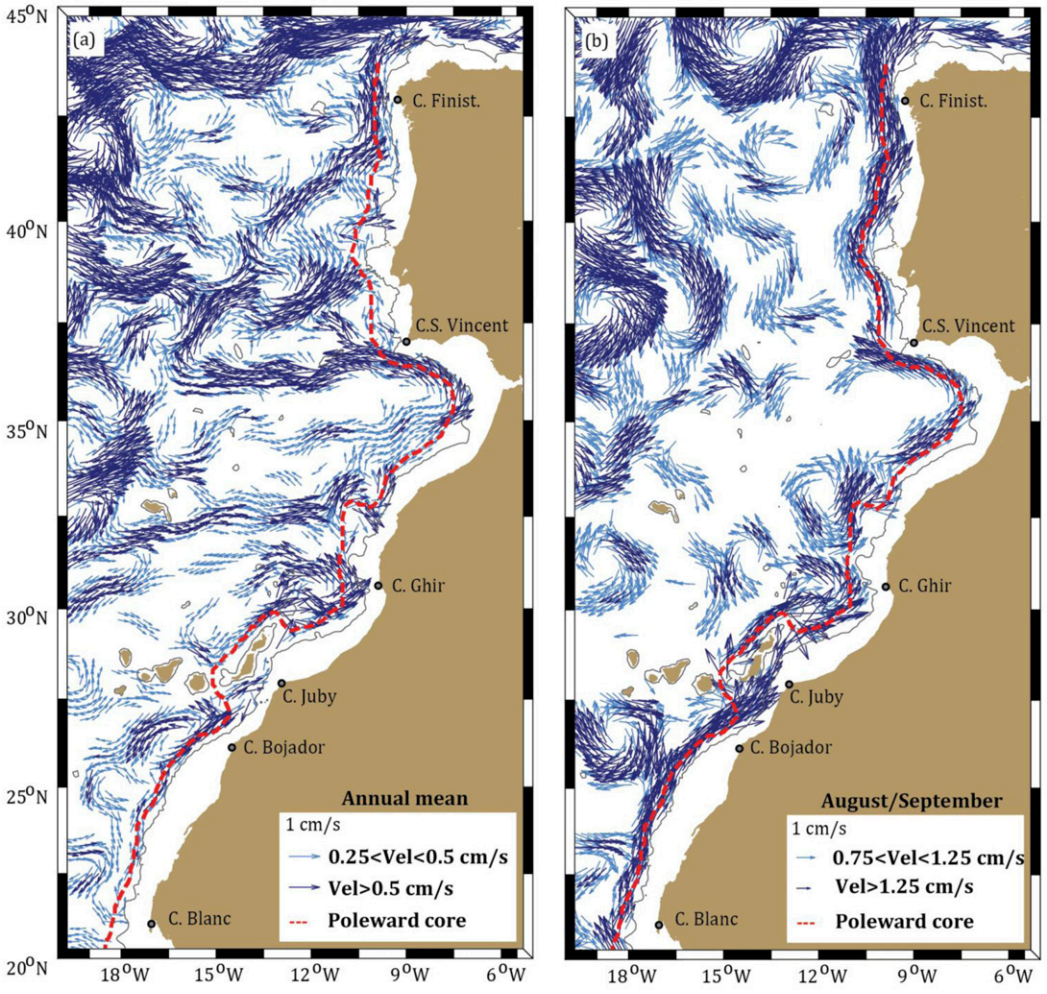


FIG. 4. Mean absolute velocities from the OFES simulation forced with QS winds at 1000 m, the parking depth of the Argo floats: (a) annual mean and (b) August and September (1 Aug–30 Sep) mean. For reference, the 1000-m isobath is represented as a gray line. Dark-gray circles show the main topographic and geographical features referred to in the text. The red dashed line denotes the core of the CiPU at 1000 dbar for the August–September mean from the OFES simulation forced with QS winds. Note the different velocity scales in the two panels.

mixing with upper Labrador Seawater at 27.75 kg $m^{-3}$ (Prieto et al. 2013) (Fig. 3b).

Although the Argo trajectories permit to establish the continuity of the CiPU from Cape Bojador to Cape Finisterre, there are not enough trajectories to establish the path of the CiPU in the overall CanCEBUS, its seasonal cycle, and the forcing mechanisms. Therefore, we have used high-resolution (0.1°) model simulations from the Ocean General Circulation Model of the Earth Simulator Center (Masumoto et al. 2004) (OFES) to further investigate the CiPU and its forcing mechanisms. Using in situ velocity observations from a 9-yr mooring in the Lanzarote Passage (Fraile-Nuez et al. 2010; Hernández-Guerra et al. 2003), we have validated the OFES high-resolution simulations in the area. The in situ velocity observations in the Lanzarote Passage show the same seasonal cycle that the OFES simulations forced with QS winds and with winds from the NCEP–NCAR reanalysis (Fig. 2). Both, the in situ observations and the model simulations, show that the maximum poleward velocities occur during the months of August and September (1 August–30 September), and the maximum equatorward velocities during the months of November and December (1 November–31 December). This high similarity between the simulations and the observations indicates that the forcing mechanism of the CiPU is well represented in the OFES simulations and that we have to look beyond the wind forcing to determine the distinctive feature among the four EBUS that results in the CiPU. The absolute velocity field at 1000 dbar from the OFES model simulations, forced with QS winds (Fig. 4), agrees with the observations from the Argo floats and confirms that there is a poleward flow at 1000 dbar, continuously from Cape Blanc (21°N) to Cape Finisterre (45°N), along the African and Iberian slopes (Fig. 4). The poleward flow is stronger and less patchy during the months of August and September. In the annual mean (Fig. 4a), south

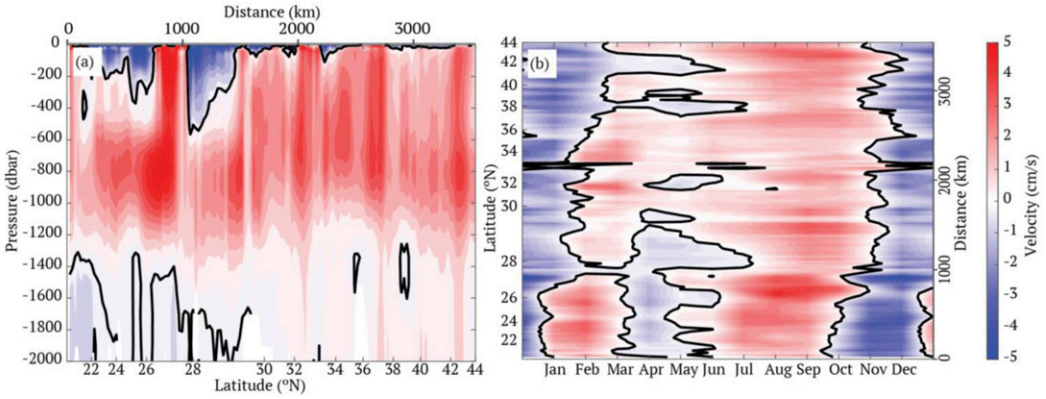


FIG. 5. Vertical section and seasonal variability of the mean velocities for the CiPU from the OFES simulation forced with QS winds: (a) vertical section of annual mean velocity along the poleward core line (red dashed line in Fig. 4) for the OFES simulations forced with QS winds, and (b) monthly mean velocity at 1000 dbar along the poleward core line (red dashed line in Fig. 4) for the OFES simulations forced with QS winds. Poleward (positive) velocities are in red, and equatorward (negative) velocities are in blue.

of 25°N, and coincident with the area without Argo poleward trajectories (Fig. 1); the poleward flow is weak except during August and September (Fig. 4b). In both average distributions, at 31°N there is a region where a discontinuity in the poleward flow is observed.

The vertical distribution of velocities along the path of the poleward flow is also consistent with the Argo trajectories, which indicates a persistent poleward flow at 1000 dbar. In the annual mean simulations (Fig. 5a), the poleward flow extends from 200 to 1400 dbar. South of 25°N the mean velocities are weaker (Fig. 5a). As the monthly percentage of Argo profiles with poleward trajectories indicates (Fig. 1b), the model simulation also shows high seasonal variability in the CiPU (Fig. 5b). The CiPU is only continuous between Cape Blanc

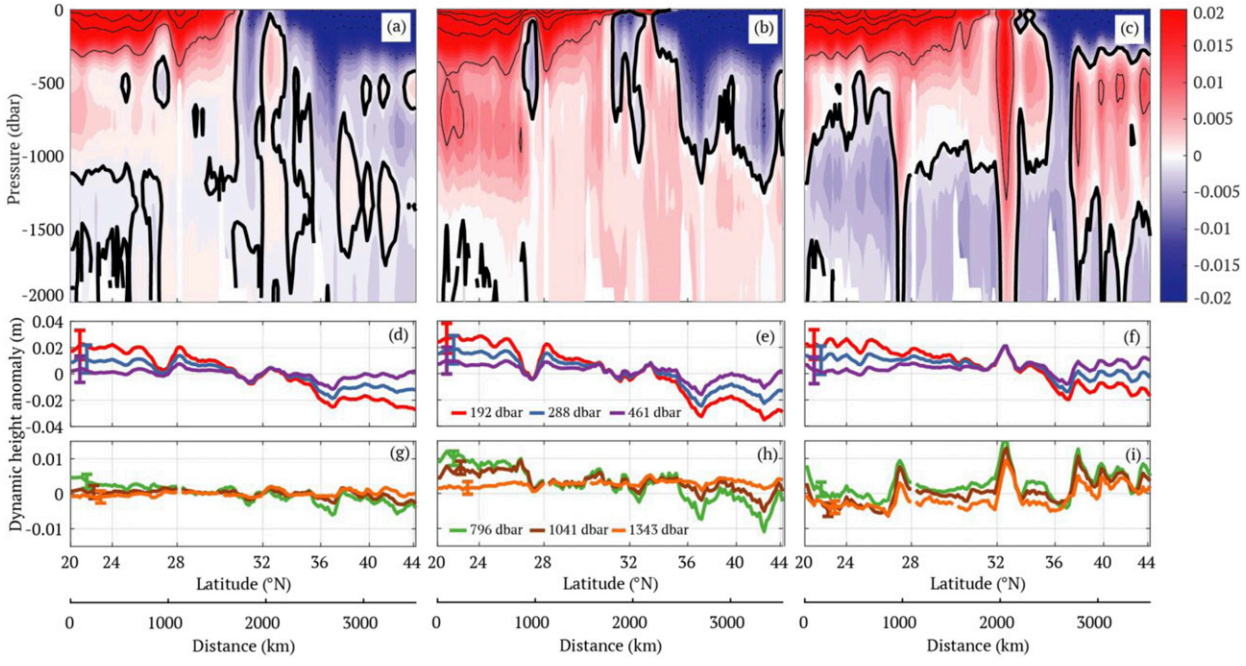


FIG. 6. Vertical sections of absolute dynamic height anomaly (mean vertical profile subtracted) from the OFES simulation forced with QS wind for the (a) annual mean, (b) August and September mean, and (c) November and December mean, with positive values in red and negative values in blue. Absolute dynamic height anomaly at selected depths for the (d)–(f) upper 500 and (g)–(i) 500–1500 dbar for the (left) annual mean, (center) August–September mean, and (right) November–December mean. The dynamic height anomaly was obtained with the OFES simulation data along the core of the CiPU line (red line in Fig. 4), using the surface as reference level and incorporating the OFES sea surface height. Uncertainties for (d)–(i) are indicated as error bars at the beginning of each line.

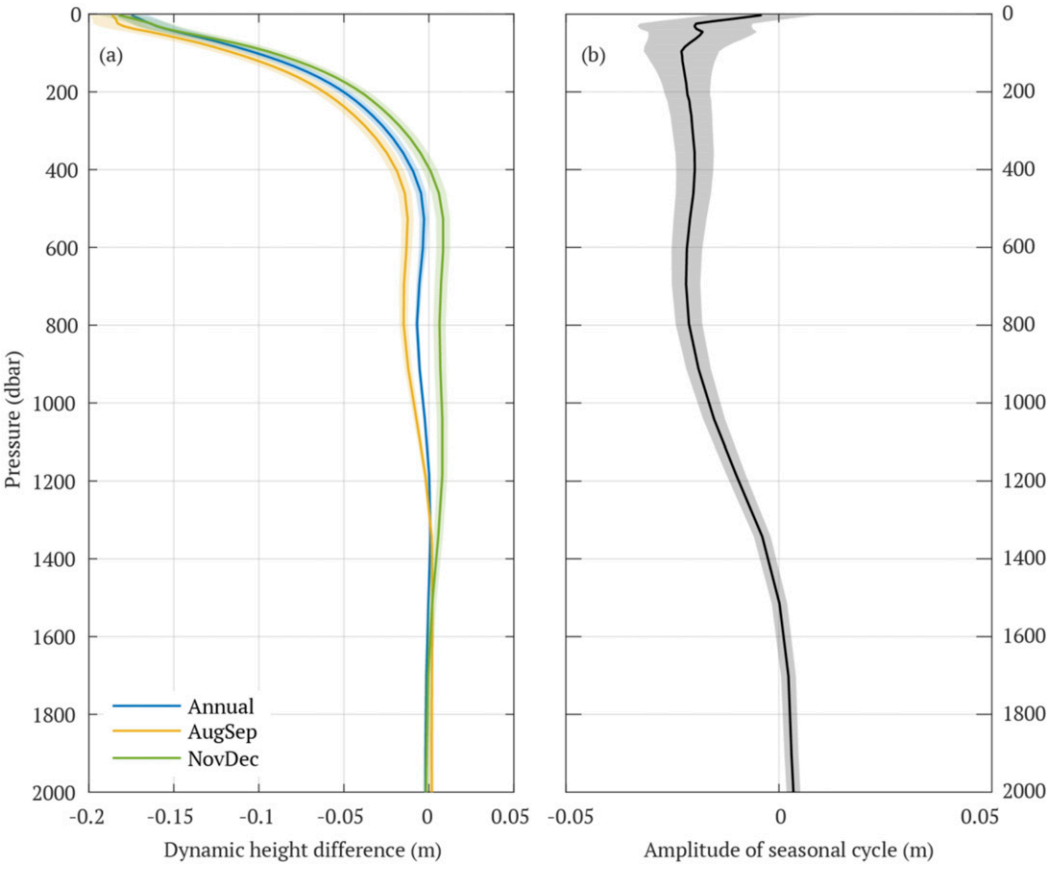


FIG. 7. (a) Profiles of absolute north–south dynamic height difference from the OFES simulation forced with QS wind, computed as the difference of the robust regression of the absolute dynamic height anomaly for each depth along the core of the CiPU, for the annual (blue), August and September (yellow), and November and December (green) means. (b) Profile of the amplitude of the seasonal cycle (mean of November and December minus mean of August and September) of the north–south absolute dynamic height in (a).

(21°N) and Cape Finisterre (43°N) from the second fortnight of July to the first fortnight of October, with maximum annual mean velocities up to $5 \pm 0.4\,\mathrm{cm\,s^{-1}}$. During November and December, there is no poleward flow. It appears again between January and March, although weaker and patchy along the coast of the Iberian Peninsula (37°–44°N), to practically disappear in spring (Fig. 5b).

### *b. Meridional alongshore pressure gradient*

Given that OFES simulations in the CanCEBUS properly represent the CiPU, we will use them to gain insight into its forcing mechanisms. The DH anomaly computed from the density and surface sea level fields in the high-resolution OFES model simulations (Fig. 6) indicates that there is an alongshore pressure gradient in the upper levels (<1500 dbar). The gradient is still observed as deep as 1041 and 796 dbar, at which depths there is an annual mean north–south DH difference of −0.3 and −0.66 cm, respectively, between 20° and 44°N (Fig. 6g). Consistent with the seasonal variability of the mean velocity at 1000 dbar, the north–south difference in DH anomaly is maximum during the months of August and September (Fig. 6h), −0.88 and −1.45 cm at 1041 and 796 dbar, respectively, between 20° and 44°N, whereas during the months of November and December the north–south DH difference (Fig. 6i) is positive. The vertical profile of the north–south difference in DH (Fig. 7a) show minimum values at the surface, with −17.5 cm of north–south DH difference for the annual mean, this is the magnitude of the north–south gradient is largest at the surface. The vertical profile of the north–south difference in DH is still negative as deep as 1200 dbar in the annual mean and 1300 dbar in the August and September mean, with a relative minimum at 800 dbar. The amplitude of the seasonal cycle in the north–south difference in DH anomaly is −2 cm from 100 to 800 dbar, and from there it decreases to 0 at 1500 dbar (Fig. 7b).

In the model simulations, the magnitude of the DH at the surface is higher than at deeper levels, but it is the density structure that allows the surface alongshore pressure gradient to propagate to deeper levels. The large-scale meridional alongshore density gradient is still observed (Fig. 8) as deep as 1041 and 796 dbar, where there is an annual mean north–south density difference of 0.02 and $0.005\,\mathrm{kg\,m^{-3}}$, respectively,

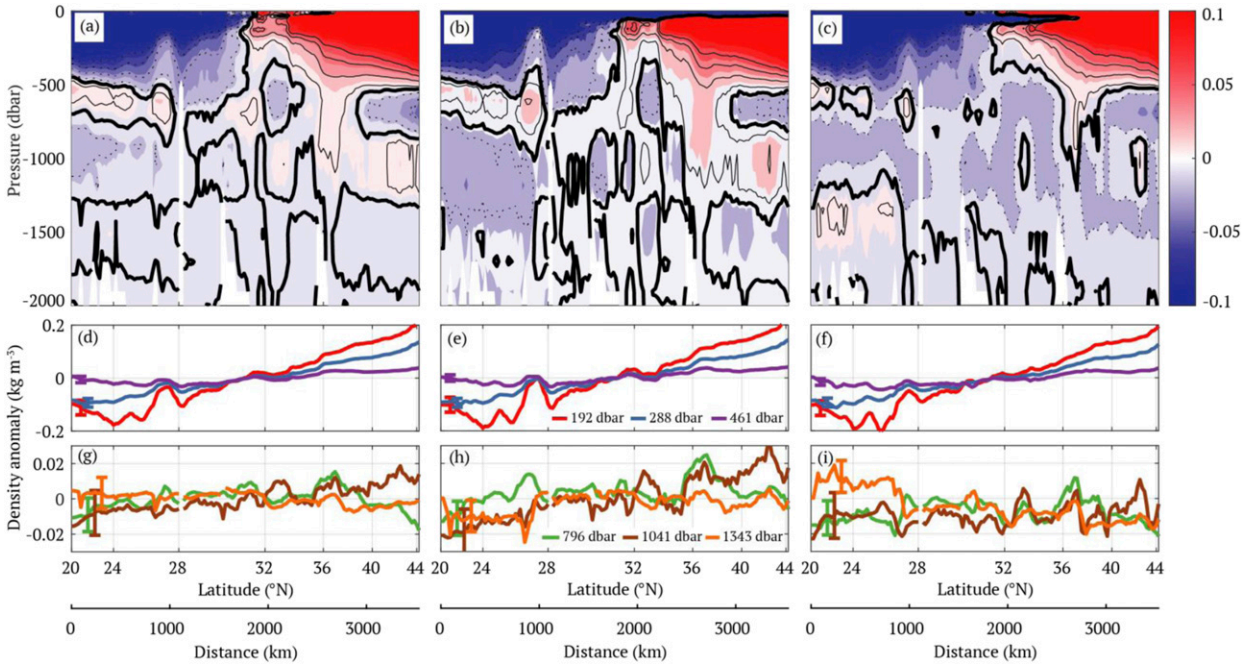


FIG. 8. Vertical sections of density anomaly (mean vertical profile subtracted) from the OFES simulation forced with QS wind for the (a) annual mean, (b) August and September mean, and (c) November and December mean, with positive and negative values in red and blue, respectively. Also shown is density anomaly at selected depths for (d)–(f) the upper 500 dbar and (g)–(i) 500–15000 dbar for the (left) annual mean, (center) August–September mean, and (right) November–December mean. The density anomaly was obtained with the OFES simulation data along the core of the CiPU line (red line in Fig. 4). Uncertainties for (d)–(i) are indicated as error bars at the beginning of each line.

between 20° and 44°N (Fig. 8g). At 1041 dbar, the north–south density difference decreases from 0.04 kg m$^{-3}$ during August and September to 0.005 kg m$^{-3}$ during November and December. The amplitude of the seasonal cycle of the north–south density difference goes from 0.8 kg m$^{-3}$ at the surface to vanish at 300 dbar, and from there it increases to a relative maximum at 1200 dbar of 0.04 kg m$^{-3}$, with positive values from 800 to 1600 dbar (Fig. 9).

In the upper levels, 200 dbar (Fig. 10), the density obtained from the high-resolution Argo-derived climatology (Roemmich and Gilson 2009) shows that, overall, all the EBUS have a similar large-scale range in density in the selected domain, although slightly larger for the CalCEBUS (Table 2). In the CalCEBUS, at 200 dbar, there is a 1.14 kg m$^{-3}$ range in density in the entire domain. However, the range in density at 200 dbar along the 1000-m isobath, used as a representative of the slope, is 0.21 kg m$^{-3}$. At a depth of 200 dbar, the CanCEBUS shows a density range of 0.62 kg m$^{-3}$ in the entire domain and 0.42 kg m$^{-3}$ along the 1000-m isobath. At 200 dbar, in the entire domain, the HumCEBUS and BenCEBUS have ranges of 0.96 and 0.55 kg m$^{-3}$, respectively, similar to those found in the CanCEBUS. The densities at 200 dbar along the slope (1000-m isobath) for the HumCEBUS and the BenCEBUS are in the same range as those for the CalCEBUS, 0.29 and 0.18 kg m$^{-3}$, respectively (Table 2).

At 1000 dbar (Fig. 11), the large-scale gradients in density are low in all the EBUS, except for the CanCEBUS. In the CanCEBUS, for the entire region, the density range is 0.21 kg m$^{-3}$ and remains of the same order of magnitude, 0.18 kg m$^{-3}$, at 1000 dbar but over the 1000-m isobath, representative of the slope. This along-slope density range is 4 times the range existing in the CalCEBUS, or 6 times the overall range in density along the slope for the HumCEBUS and the BenCEBUS. At 1000 dbar the density range for the CalCEBUS has decreased considerably, becoming the EBUS with the lowest full-area density range.

The meridional alongshore density gradient in the CanCEBUS at 1000 dbar, over the slope (1000-m isobath), is explained by the difference between the light, fresh, and cold AAIW in the south, and the dense, salty, and warm MOW in the north. In the other EBUSs, there is not an appreciable difference in water masses below 1000 dbar, and therefore the distribution of density at 1000 dbar is almost homogenous. The vertical penetration of the meridional APG allowed by this meridional alongshore density gradient permits the development of a poleward undercurrent (800–1000 dbar) in the CanCEBUS, deeper than in the other EBUS (400 dbar).

## 4. Discussion and conclusions

Poleward undercurrents are well-known features in eastern boundary upwelling systems. However, in the Canary Current upwelling system, the CiPU has not been properly characterized. Our results indicate that the CiPU, the poleward flow

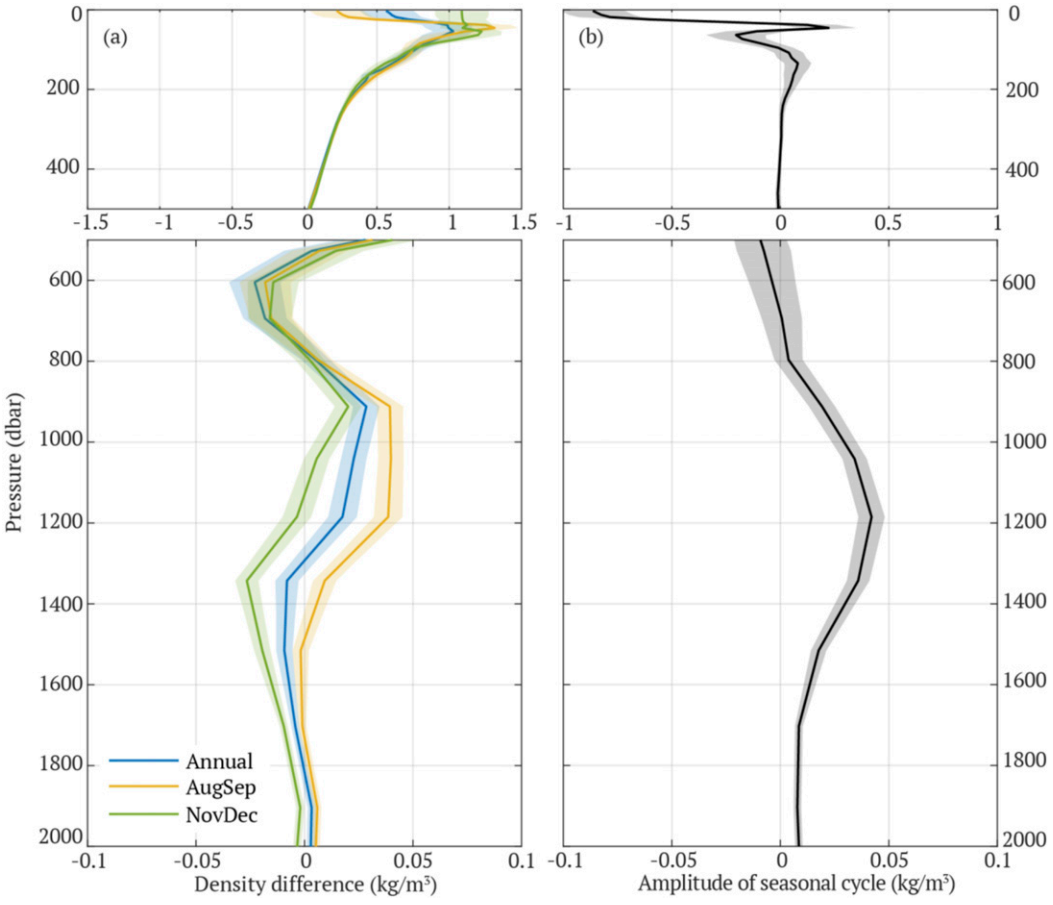


FIG. 9. (a) Profiles of absolute north–south density difference from the OFES simulation forced with QS wind, computed as the difference of the robust regression of the density for each depth along the core of the CiPU, for the annual (blue), August and September (yellow), and November and December (green) means. (b) Profile of the amplitude of the seasonal cycle (mean of November and December minus mean of August and September) of the north–south density (a). Note the different *x* axis for the upper 500 dbar in both (a) and (b).

in the CanCEBUS, is a robust and persistent feature, with its core at 1000 dbar. It is driven by the meridional APG created by the large-scale ocean, including wind-driven, circulation, that penetrates up to 1000 dbar due to the density gradient between the light, fresh and cold AAIW in the south, and the dense, salty and warm MOW in the north.

Argo trajectories at 1000 dbar (Fig. 1) show that the poleward flow in the CanCEBUS is continuous along the slope of north Africa and the Iberian Peninsula, extending from south of Cape Bojador (26°N) to the northwest coast of Spain, north of Cape Finisterre (44°N). We found that 53 Argo floats returned to the CiPU after surfacing every 10 days, spending more than 12 h between ascending and at the surface. The same analysis performed for the CanCEBUS was carried out for the other three EBUS, with the same range of latitude and longitude. Despite a similar total number of Argo floats in the four EBUS, only the CanCEBUS shows a robust and persistent poleward flow at 1000 dbar. Although the observations are limited to the coverage of the Argo data until March 2018, these results are consistent with the wide range of observations in the CalCEBUS (Collins et al. 2018; Todd et al. 2011), but also with the more limited dataset in the HumCEBUS (Fonseca 1989) and the BenCEBUS (Benitez-Nelson et al. 2007) that indicate that the core of the poleward flow in these EBUS is not at 1000 dbar (Neshyba et al. 1989).

The CTD observations from the Argo floats indicate that south of Cape Ghir the CiPU advects AAIW, while as it progresses poleward, the CiPU advects mixed MOW. The steep topography in the area of the Cape Ghir allows to develop mesoscale activity (Sangrà et al. 2015), as a semipermanent upwelling filament, that forces the poleward flow to meander. It is in this region where it is observed a discontinuity in the transition between the AAIW and the MOW. These results are consistent with long time series of hydrographic properties and velocity observations in the Lanzarote passage (Fraile-Nuez et al. 2010; Pérez-Hernández et al. 2015; Machín and Pelegrí 2009), the observations at the exit of the Gibraltar Strait (Zenk and Armi 1990; Mittelstaedt 1983) and the observations along the Iberian Peninsula that indicate poleward flow at the level of the MOW almost all year long, but

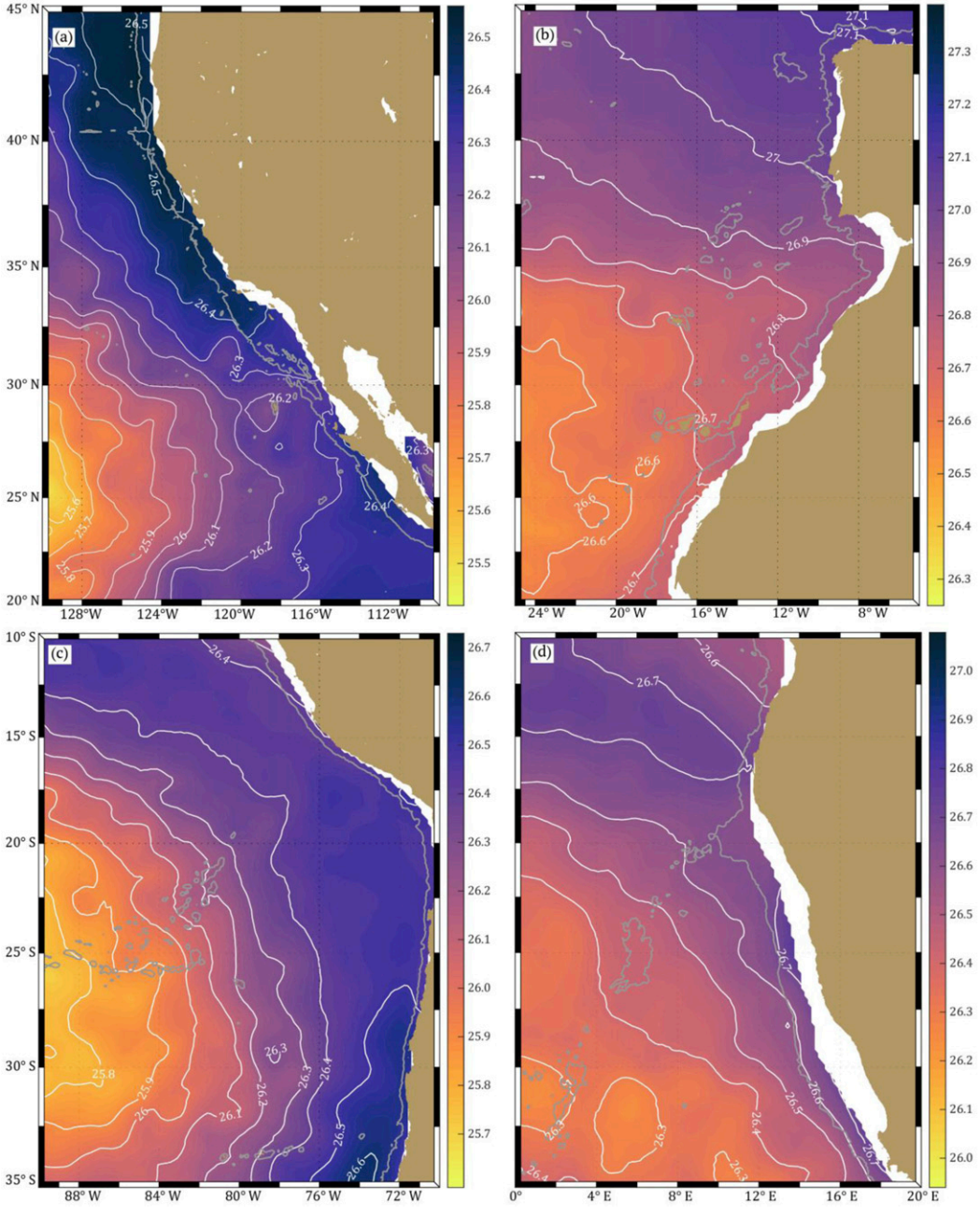


FIG. 10. Horizontal density distribution in the four EBUSs from the Argo-derived temperature and salinity climatology (Roemmich and Gilson 2009): density at 200 dbar for the (a) California, (b) Canary, (c) Humboldt, and (d) Benguela Current eastern boundary upwelling systems. Note that the range in the color scale is the same for the four regions, 1.14 kg m$^{-3}$, although the interval is different for each EBUS as described in Table 2. White contours appear each 0.1 kg m$^{-3}$. The latitudinal band and the range in longitude are the same for all of the regions. The gray line marks the 2000-m isobath.

decreasing or even reversing in November (Teles-Machado et al. 2016).

To further characterize the CiPU, we used the OFES ocean model simulations. The model is in good agreement with long-term mooring observations in the Lanzarote Passage (Fraile-Nuez et al. 2010), and with the poleward flow observed with the Argo floats. In the model, the CiPU is also a persistent and robust poleward undercurrent flowing along the slopes of North Africa and the Iberian Peninsula, with a mean velocity of 5 cm s$^{-1}$ and with its core located between 800 and 1000 dbar. The model simulations are consistent with previous modeling studies that found a poleward undercurrent between

TABLE 2. Ranges (max − min) of the density fields in the four EBUS at 200 and 1000 dbar in the domain of Figs. 10 and 11. In parentheses in the second and fourth columns are the along-slope density ranges using the 1000-m isobath as representative of the slope. The intervals in the third column, at 1000 dbar, are those used in Figs. 10 and 11.

| | Interval at 200 dbar [min; max] ($kg\,m^{-3}$) | Range at 200 dbar ($kg\,m^{-3}$) | Interval at 1000 dbar [min; max] ($kg\,m^{-3}$) | Range at 1000 dbar ($kg\,m^{-3}$) |
|---|---|---|---|---|
| CalCEBUS | [25.42; 26.56] | 1.14 (0.21) | [27.30; 27.40] | 0.10 (0.04) |
| CanCEBUS | [26.51; 27.14] | 0.62 (0.42) | [27.48; 27.69] | 0.21 (0.18) |
| HumCEBUS | [25.68; 26.64] | 0.96 (0.29) | [27.25; 27.38] | 0.13 (0.03) |
| BenCEBUS | [26.24; 26.79] | 0.55 (0.18) | [27.23; 27.46] | 0.23 (0.03) |

1000 and 1400 dbar between Cape Ghir and the Iberian Peninsula (Batteen et al. 2000, 2007; Mason et al. 2011). The OFES model simulations allow us to establish the alongshore pressure gradient as the main driving mechanism for the mean structure of the CiPU.

Hill et al. (1998) and Connolly et al. (2014) proposed three hypotheses to explain the poleward flows of the eastern boundaries. The first one explains the poleward flow as an integral part of the upwelling system: the poleward flow is forced by an alongshore pressure gradient created by the along-slope variations in topography and wind strength (McCreary 1981). In the second hypothesis, a large-scale meridional APG originated in the open ocean forces the development of the poleward current. The third hypothesis links poleward undercurrents with coastally trapped waves, and the poleward flow is associated with the rectification, over the sloping boundary, of the change, in time, of the forcing. In the first two hypotheses, the driving mechanism of the poleward undercurrent is the alongshore pressure gradient, either created by the wind, the general ocean circulation, or by a large-scale poleward decrease in temperature and sea surface height. Hill et al. (1998) recognized that it is still undetermined contribution between the three forcing mechanisms described above to the driving mechanisms of the poleward undercurrent.

In this study, we used two model simulations, forced by QS and NCEP–NCAR reanalysis winds, and both of them show high similarity with the observations. The two wind forcings have an overall similar large-scale pattern, but different resolutions, with the QS winds solving small-scale features. The lack of sensitivity of the modeled CiPU to the change in the wind forcing suggests that one should look beyond the wind forcing to determine the distinctive feature among the four EBUS that results in the CiPU.

Going beyond the wind forcing permits one to rule out the first and third hypothesis proposed by Hill et al. (1998) while focusing in the second hypothesis, associated with the large-scale meridional alongshore pressure gradient. This gradient is due to the meridional decrease in the DH, caused by a decrease, mainly, in the ocean temperatures poleward (Huthnance 1984, 1995), or by the general ocean circulation forced by the wind. In the case of the CanCEBUS, our results show that even at 1000 dbar there is a meridional APG, as indicated by the DH anomaly. Since this large-scale pressure gradient is created in the open ocean, the steep continental slope isolates the shelf from the open ocean pressure influence (Wang 1982) and the CiPU does not strengthen upstream (Fig. 5b). This discards too the JEBAR as a driving mechanism (Huthnance 1984).

The meridional APG driving the CiPU is due to large-scale ocean circulation, since the sea surface height is already forcing the poleward flow and its magnitude is much larger than the DH at any deeper level (Fig. 8a). However, the density contrast between two intermediate water masses, the MOW and the AAIW, allows the surface-imposed meridional APG to penetrate to deeper levels. The distribution of density at 1000 dbar from the Argo derived climatology (Roemmich and Gilson 2009) shows this density gradient at depth, which is unique in the four EBUS (Fig. 11).

The distribution of observations of Argo floats in the CanCEBUS (Fig. 1) shows a high seasonal cycle in the CiPU, with the maximum percentage of poleward trajectories between August and October, and minimum between March and April. Several factors can contribute to this seasonal cycle, as a seasonal change in the depth of the CiPU core, the distribution of the number of floats, or a seasonal change in the strength of the CiPU. However, the OFES simulations corroborated this seasonal cycle observed in the Argo floats. We have explained that the forcing mechanism of the CiPU is the alongshore pressure gradient imposed by the general ocean circulation, while the contrast between the MOW and the AAIW allows this alongshore pressure gradient to propagate deeper than 1200 dbar. However, the properties of these water masses do not change seasonally, and therefore the causes of the seasonal variability observed are still unknown. The vertical evolution of the pressure gradient as a function of depth and the season (Fig. 7) shows that the amplitude of the seasonal cycle has a relative maximum at 800 dbar, and then it decreases to vanish at 1600 dbar, suggesting that the seasonal variability is not only due to the seasonal variability at the surface. Moreover, the density differences (Figs. 8 and 9) show that there is a seasonal cycle from 800 to 1400 dbar, with the maximum differences in density during August and September. The density differences in the upper 200 dbar have a different seasonal cycle, with minimum differences in density during August and September, and therefore indicating that the interaction of the MOW and AAIW plays a key role in the seasonal cycle of the CiPU.

Since the CiPU advects AAIW poleward, mixing it with the MOW, the seasonal variability should be related to the renewal of the AAIW; otherwise, the advection of AAIW by the CiPU will destroy the meridional alongshore density gradient that allows the alongshore pressure gradient to penetrate deeper than 1000 dbar.

Previous authors (Machín and Pelegrí 2009) suggest that Ekman pumping can start the poleward flow of AAIW by

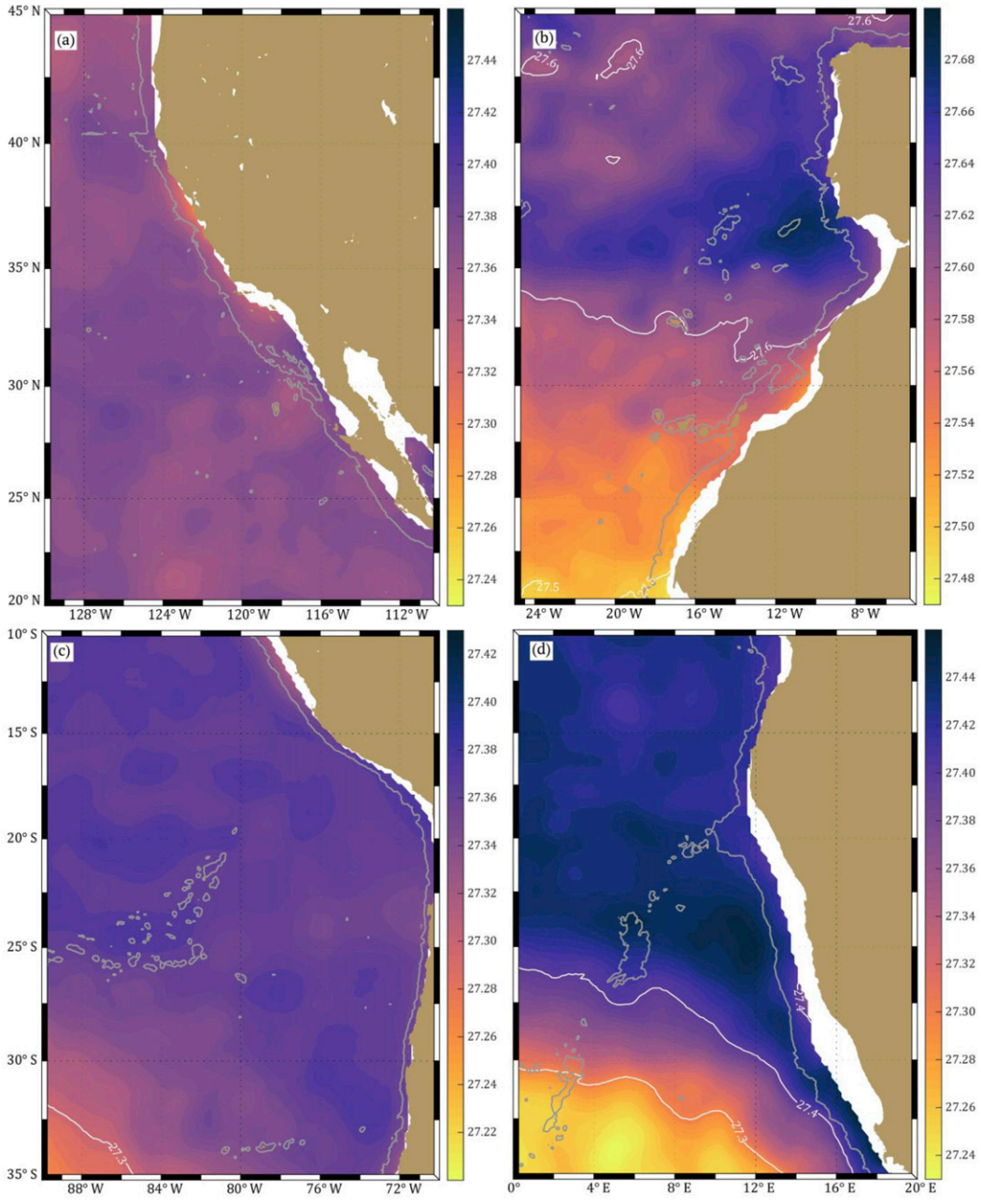


FIG. 11. Horizontal density distribution in the four EBUSs from the Argo-derived temperature and salinity climatology (Roemmich and Gilson 2009). Density at 1000 dbar for the (a) California, (b) Canary, (c) Humboldt, and (d) Benguela Current eastern boundary upwellings. Note that the range in the color scale is the same for the four regions, 0.23 kg $m^{-3}$, although the interval is different for each EBUS as described in Table 2. White contours appear each 0.1 kg $m^{-3}$. The latitudinal band and the range in longitude are the same for all of the regions. The gray line marks the 2000-m isobath.

Ekman suction of purer AAIW from the tropics (Fratantoni and Richardson 1999) (Fig. 12a). The seasonal cycle of the wind stress curl in the tropical region near Cape Blanc is stronger between March and October (Fig. 12b), while in the other regions the seasonal cycle is characterized by a pronounced peak in a given season of the year. The seasonal cycle of the wind stress curl near Cape Blanc is closely related to the seasonal cycle of the CiPU at the Lanzarote Passage (Fig. 12c). Given that in the tropical regions the AAIW gets shallow enough to be affected by Ekman suction (Machín and Pelegrí 2009), the increase in the wind stress curl in Cape Blanc, from March to October provides enough suction to

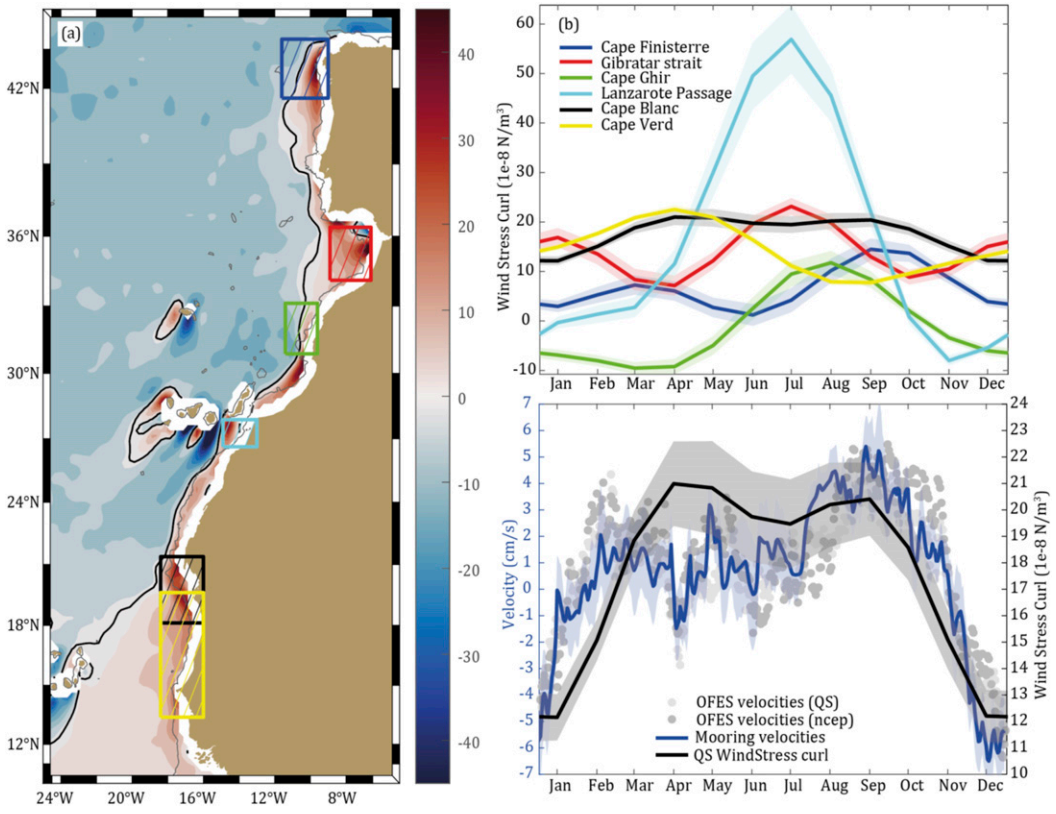


FIG. 12. Wind stress curl along the CanCEBUS. (a) Annual mean wind stress curl in the CanCEBUS obtained from the Scatterometer Climatology of Ocean Winds (Risien and Chelton 2008). The outlined boxes indicate the areas used in (b), (b) Seasonal cycle of wind stress curl ($1 \times 10^{-8}$ N m$^{-3}$) in the areas indicated in (a). The same color code was used to identify the areas in both panels, (c) The black line is the seasonal cycle of wind stress curl in the Cape Blanc area, the black box in (a), centered at 17.44°W, 19.42°N. The blue line is the seasonal cycle of the rotated velocity from the current meter at 870 m of the long-term mooring located in the Lanzarote Passage (Fraile-Nuez et al. 2010; Hernández-Guerra et al. 2003), as in Fig. 3. The light-gray and dark-gray dots correspond to the rotated velocity from the OFES simulations forced with QuikSCAT and NCEP–NCAR reanalysis winds, respectively, at the same location and depth of the mooring data. The velocities were rotated to the principal axis of the mooring observations at 870 dbar (51.2° clockwise).

incorporate AAIW from the tropical Atlantic into the slope (Fratantoni and Richardson 1999; Hernández-Guerra et al. 2005). The accumulated suction of AAIW from March to September builds up the meridional alongshore density gradient that is stronger in August and September, as the CiPU.

However, understanding the seasonal cycle of the CiPU is not only relevant for the regional ocean circulation in the CanCEBUS. The mean strength of the AMOC is, as estimated, among others, by with the RAPID-MOCHA array, 18.7 Sv (McCarthy et al. 2015; Hernández-Guerra et al. 2014). Its seasonal cycle is 6.7 Sv, with a 5.9-Sv contribution from the upper ocean to midocean and the maximum in autumn and minimum in spring (Kanzow et al. 2010). Recent studies with RAPID-MOCHA data argue that the ocean dynamics of the eastern subtropical Atlantic is the main driver for this seasonal cycle of the AMOC, and Vélez-Belchí et al. (2017) demonstrated than the recirculation of the Canary Current and the seasonal cycle of the CiPU explain the seasonal cycle of the AMOC as observed by the RAPID-MOCHA array (Vélez-Belchí et al. 2017; Hernández-Guerra et al. 2017).

The seasonal cycle in the eastern subtropical Atlantic is in phase with the seasonal cycle of the AMOC, which requires the smallest contribution to the upper- to midocean to be in autumn since the AMOC has its maximum poleward transport in autumn. The CiPU contributes to the seasonal cycle of the subtropical eastern Atlantic with a seasonal cycle in the range from 2.8 ± 0.4 to 7.6 ± 0.6 Sv (Casanova-Masjoan et al. 2020; Vélez-Belchí et al. 2017; Hernández-Guerra et al. 2002), and, as we have demonstrated here, this seasonal cycle is mainly related to the seasonal cycle of the wind in the subtropical southeastern Atlantic.

In summary, the CiPU is driven by the meridional APG associated with the large-scale ocean and wind-driven circulation that penetrates deeper than 1000 dbar as a result of the presence of the AAIW and the MOW. The CiPU flows deeper (1000 dbar) than any other eastern boundary

poleward undercurrent, with a high seasonal variability that is due to the poleward extension of AAIW, forced by Ekman pumping in the tropics. Understanding the CiPU and its driving mechanisms is important to evaluate its role in maintaining the productivity of the CanCEBUS, but also to assess the role of the eastern Atlantic Ocean in the seasonal cycle of the AMOC.

*Acknowledgments.* This study has been carried out as part of the RAPROCAN Project, the Canary Islands component of the core observational program of the Instituto Español de Oceanografía; the SAGA project (RTI2018-100844-B-C32), funded by the Ministerio de Economía y Competividad; the EA-RISE (Euro-Argo Research Infrastructure Sustainability and Enhancement) project, funded by European Union's Horizon 2020 research and innovation program under Grant Agreement H2020-INFRADEV-2018-2020824131); and BOUNDARY (ProID2017010083), funded by PO Feder Canarias. Author Caínzos thanks the Agencia Canaria de Investigación, Innovación y Sociedad de la Información (ACIISI) for grant Apoyo al Personal Investigador en Formación. Arumí-Planas, Santana Toscano, and Caínzos are Ph.D. students in the IOCAG Doctoral Program in Oceanography and Global Change. Author Pérez-Hernández is funded through the postdoctoral program of the University of Las Palmas de Gran Canaria. The model data were provided by Asia-Pacific Data Research Center, which is a part of the International Pacific Research Center at the University of Hawai'i at Mānoa, funded in part by the National Oceanic and Atmospheric Administration (NOAA). The color maps in Figs. 3, 10, and 11 are from the cmocean toolbox provided by Thyng et al. (2016). The maps in Figs. 1, 3, 10, 11, and 12 use the set of mapping tools written by Pawlowicz (2020). The Argo data are collected and made freely available by the International Argo Program and the national programs that contribute to it (http://www.argo.ucsd.edu, http://argo.jcommops.org). The Argo Program is part of the Global Ocean Observing System. Sadly for us, and unexpectedly, Maria Casanova-Masjoan died on 15 October 2020. She was a Ph.D. student in the IOCAG Doctoral Program in Oceanography and Global Change, and this work is dedicated to her memory. Maria was a great scientist, great colleague, and great friend.

*Data availability statement.* OFES data are available through http://apdrc.soest.hawaii.edu/dods/public_ofes/OfES, Argo data are available through ftp://ftp.ifremer.fr/ifremer/argo, and Argo derived climatology (Roemmich and Gilson 2009) is available through http://sio-argo.ucsd.edu/RG_Climatology.html.

## REFERENCES

Antonov, J. I., R. A. Locarnini, T. P. Boyer, A. V. Mishonov, and H. E. Garcia, 2006: *Salinity*. Vol. 2, *World Ocean Atlas 2005*, NOAA Atlas NESDIS 62, 182 pp.

Argo, 2019: Argo float data and metadata from Global Data Assembly Centre (Argo GDAC)—Snapshot of Argo GDAC of December 10th 2019. Argo, accessed 16 December 2019, https://doi.org/10.17882/42182#68867.

Baker-Yeboah, S., D. A. Byrne, and D. R. Watts, 2010: Observations of mesoscale eddies in the South Atlantic Cape Basin: Baroclinic and deep barotropic eddy variability. *J. Geophys. Res.*, **115**, C12069, https://doi.org/10.1029/2010JC006236.

Barton, E. D., 1989: The poleward undercurrent on the eastern boundary of the subtropical North Atlantic. *Poleward Flows Along Eastern Ocean Boundaries*. S. Neshyba et al., Eds., Coastal and Estuarine Studies, Vol. 34, Springer, 82–95.

Batteen, M. L., J. R. Martinez, D. W. Bryan, and E. J. Buch, 2000: A modeling study of the coastal eastern boundary current system off Iberia and Morocco. *J. Geophys. Res.*, **105**, 14 173–14 195, https://doi.org/10.1029/2000JC900026.

——, A. S. Martinho, H. A. Miller, and J. L. McClean, 2007: A process-oriented modelling study of the coastal Canary and Iberian Current system. *Ocean Modell.*, **18**, 1–36, https://doi.org/10.1016/j.ocemod.2007.02.006.

Benitez-Nelson, C. R., and Coauthors, 2007: Mesoscale eddies drive increased silica export in the subtropical Pacific Ocean. *Science*, **316**, 1017–1021, https://doi.org/10.1126/science.1136221.

Casanova-Masjoan, M., M. D. Pérez-Hernández, P. Vélez-Belchí, L. Cana, and A. Hernández-Guerra, 2020: Variability of the Canary Current diagnosed by inverse box models. *J. Geophys. Res. Oceans*, **125**, e2020JC016199, https://doi.org/10.1029/2020JC016199.

Chidichimo, M. P., T. Kanzow, S. A. Cunningham, W. E. Johns, and J. Marotzke, 2010: The contribution of eastern-boundary density variations to the Atlantic meridional overturning circulation at 26.5°N. *Ocean Sci.*, **6**, 475–490, https://doi.org/10.5194/os-6-475-2010.

Collins, C. A., N. Garfield, R. G. Paquette, and E. Carter, 1996: Lagrangian measurement of subsurface poleward flow between 38°N and 43°N along the West Coast of the United States during summer, 1993. *Geophys. Res. Lett.*, **23**, 2461–2464, https://doi.org/10.1029/96GL02138.

——, ——, T. A. Rago, F. W. Rischmiller, and E. Carter, 2000: Mean structure of the inshore countercurrent and California undercurrent off Point Sur, California. *Deep-Sea Res. II*, **47**, 765–782, https://doi.org/10.1016/S0967-0645(99)00126-5.

——, J. T. Pennington, C. G. Castro, T. A. Rago, and F. P. Chavez, 2003: The California Current system off Monterey, California: Physical and biological coupling. *Deep-Sea Res. II*, **50**, 2389–2404, https://doi.org/10.1016/S0967-0645(03)00134-6.

——, L. M. Ivanov, O. V. Melnichenko, and N. Garfield, 2004: California undercurrent variability and eddy transport estimated from RAFOS float observations. *J. Geophys. Res.*, **109**, C05028, https://doi.org/10.1029/2003JC002191.

——, T. A. Rago, T. Margolina, and L. Ivanov, 2018: Lagrangian observations of the along-slope path of the California undercurrent. *Deep-Sea Res. II*, **151**, 115–128, https://doi.org/10.1016/j.dsr2.2018.04.010.

Connolly, T. P., B. M. Hickey, I. Shulman, and R. E. Thomson, 2014: Coastal trapped waves, alongshore pressure gradients, and the California Undercurrent. *J. Phys. Oceanogr.*, **44**, 319–342, https://doi.org/10.1175/JPO-D-13-095.1.

Fiuza, A., 1982: The Portuguese coastal upwelling system. *Actual Problems of Oceanography in Portugal*, Junta Nacional de Investigação, 45–71.

Fonseca, T. R., 1989: An overview of the poleward undercurrent and upwelling along the Chilean Coast. *Poleward Flows along Eastern Ocean Boundaries*, S. J. Neshyba et al., Eds., Coastal and Estuarine Studies, Vol. 34, Amer. Geophys. Union, 203–228.

Fraile-Nuez, E., F. Machín, P. Vélez-Belchí, F. López-Laatzen, V. Benítez-Barrios, and A. Hernández-Guerra, 2010: Nine years of mass transport data in the eastern boundary of the

North Atlantic Subtropical Gyre. *J. Geophys. Res.*, **115**, C09009, https://doi.org/10.1029/2010JC006161.

Fratantoni, D. M., and P. Richardson, 1999: SOFAR float observations of an intermediate-depth eastern boundary current and mesoscale variability in the eastern tropical Atlantic Ocean. *J. Phys. Oceanogr.*, **29**, 1265–1278, https://doi.org/10.1175/1520-0485(1999)029<1265:SFOOAI>2.0.CO;2.

Garfield, N., C. A. Collins, R. G. Paquette, and E. Carter, 1999: Lagrangian exploration of the California Undercurrent, 1992–95. *J. Phys. Oceanogr.*, **29**, 560–583, https://doi.org/10.1175/1520-0485(1999)029<0560:LEOTCU>2.0.CO;2.

Hagen, E., 2001: Northwest African upwelling scenario. *Oceanol. Acta*, **24**, 113–128, https://doi.org/10.1016/S0399-1784(00)01110-5.

Haynes, R., and E. D. Barton, 1990: A poleward flow along the Atlantic coast of the Iberian Peninsula. *J. Geophys. Res.*, **95**, 11 425–11 441, https://doi.org/10.1029/JC095iC07p11425.

Hernández-Guerra, A., F. López-Laatzen, F. Machín, D. De Armas, and J. L. Pelegrí, 2001: Water masses, circulation and transport in the eastern boundary current of the North Atlantic subtropical gyre. *Sci. Mar.*, **65**, 177–186, https://doi.org/10.3989/scimar.2001.65s1177.

——, and Coauthors, 2002: Temporal variability of mass transport in the Canary Current. *Deep-Sea Res. II*, **49**, 3415–3426, https://doi.org/10.1016/S0967-0645(02)00092-9.

——, E. Fraile-Nuez, R. Borges, F. López-Laatzen, P. Vélez-Belchí, G. Parrilla, and T. Muller, 2003: Transport variability in the Lanzarote passage (eastern boundary current of the North Atlantic subtropical gyre). *Deep-Sea Res. I*, **50**, 189–200, https://doi.org/10.1016/S0967-0637(02)00163-2.

——, ——, F. López-Laatzen, A. Martínez, G. Parrilla, and P. Vélez-Belchí, 2005: Canary Current and North Equatorial Current from an inverse box model. *J. Geophys. Res.*, **110**, C12019, https://doi.org/10.1029/2005JC003032.

——, J. L. Pelegrí, E. Fraile-Nuez, V. Benítez-Barrios, M. Emelianov, M. D. Pérez-Hernández, and P. Vélez-Belchí, 2014: Meridional overturning transports at 7.5N and 24.5N in the Atlantic Ocean during 1992-93 and 2010-11. *Prog. Oceanogr.*, **128**, 98–114, https://doi.org/10.1016/j.pocean.2014.08.016.

——, E. Espino-Falcón, P. Vélez-Belchí, M. Dolores Pérez-Hernández, A. Martínez Marrero, and L. Cana, 2017: Recirculation of the Canary Current in fall 2014. *J. Mar. Syst.*, **174**, 25–39, https://doi.org/10.1016/j.jmarsys.2017.04.002.

Hill, A. E., 1998: Buoyancy effects in coastal and shelf seas. *The Global Coastal Ocean: Processes and Methods*, K. H. Brink and A. R. Robinson, Eds., *The Sea—Ideas and Observations on Progress in the Study of the Seas*, Vol. 10, John Wiley and Sons, 21–62.

Hill, E. A., B. M. Hickey, F. A. Shillington, P. T. Strub, K. H. Brink, E. D. Barton, and A. C. Thomas, 1998: Eastern ocean boundaries. *The Global Coastal Ocean: Regional Studies and Syntheses*, A. R. Robinson and K.H. Brink, Eds., *The Sea—Ideas and Observations on Progress in the Study of the Seas*, Vol. 11, John Wiley and Sons, 29–67.

Huthnance, J. M., 1984: Slope currents and "JEBAR." *J. Phys. Oceanogr.*, **14**, 795–810, https://doi.org/10.1175/1520-0485(1984)014<0795:SCA>2.0.CO;2.

——, 1995: Circulation, exchange and water masses at the ocean margin: The role of physical processes at the shelf edge. *Prog. Oceanogr.*, **35**, 353–431, https://doi.org/10.1016/0079-6611(95)80003-C.

Huyer, A., 1989: Poleward flow along eastern boundaries: What next? *Poleward Flows along Eastern Ocean Boundaries*, S. J. Neshyba et al., Eds., Springer, 40–44.

——, P. M. Kosro, S. J. Lentz, and R. C. Beardsley, 1989: Poleward flow in the California Current System. *Poleward Flows along Eastern Ocean Boundaries*, S. J. Neshyba et al., Eds., Springer, 142–159.

Kanzow, T., and Coauthors, 2010: Seasonal variability of the Atlantic meridional overturning circulation at 26.5°N. *J. Climate*, **23**, 5678–5698, https://doi.org/10.1175/2010JCLI3389.1.

Kersalé, M., and Coauthors, 2019: Shallow and deep eastern boundary currents in the South Atlantic at 34.5°S: Mean structure and variability. *J. Geophys. Res. Atmos.*, **124**, 1634–1659, https://doi.org/10.1029/2018JC014554.

Laiz, I., J. L. Pelegrí, F. Machín, P. Sangrà, A. Hernández-Guerra, A. Marrero-Díaz, and A. Rodríguez-Santana, 2012: Eastern boundary drainage of the North Atlantic subtropical gyre. *Ocean Dyn.*, **62**, 1287–1310, https://doi.org/10.1007/s10236-012-0560-6.

Lebedev, K., H. Yoshinari, N. Maximenko, and P. Hacker, 2007: YoMaHa'05: Velocity data assessed from trajectories of Argo floats at parking level and at the sea surface. IPRC Tech. Note, 16 pp., http://apdrc.soest.hawaii.edu/projects/yomaha/.

Locarnini, R. A., A. V. Mishonov, J. I. Antonov, T. P. Boyer, and H. E. Garcia, 2006: *Temperature*. Vol. 1, *World Ocean Atlas 2005*, NOAA Atlas NESDIS 61, 182 pp.

Machín, F., and J. L. Pelegrí, 2009: Northward penetration of Antarctic intermediate water off Northwest Africa. *J. Phys. Oceanogr.*, **39**, 512–535, https://doi.org/10.1175/2008JPO3825.1.

——, ——, E. Fraile-Nuez, P. Vélez-Belchí, F. López-Laatzen, and A. Hernández-Guerra, 2010: Seasonal flow reversals of intermediate waters in the Canary Current System East of the Canary Islands. *J. Phys. Oceanogr.*, **40**, 1902–1909, https://doi.org/10.1175/2010JPO4320.1.

Mason, E., F. Colas, J. Molemaker, A. F. Shchepetkin, C. Troupin, J. C. McWilliams, and P. Sangrà, 2011: Seasonal variability of the Canary Current: A numerical study. *J. Geophys. Res.*, **116**, C06001, https://doi.org/10.1029/2010JC006665.

Masumoto, Y., and Coauthors, 2004: A fifty-year eddy-resolving simulation of the world ocean: Preliminary outcomes of OFES (OGCM for the Earth Simulator). *J. Earth Simul.*, **1**, 35–36.

McCarthy, G. D., D. A. Smeed, and W. E. Johns, 2015: Measuring the Atlantic meridional overturning circulation at 26°N. *Prog. Oceanogr.*, **130**, 91–111, https://doi.org/10.1016/j.pocean.2014.10.006.

McCreary, J. P., 1981: A linear stratified ocean model of the coastal undercurrent. *Philos. Trans. Roy. Soc. London*, **302A**, 385–413, https://doi.org/10.1098/rsta.1981.0176.

——, S. R. Shetye, and P. K. Kundu, 1986: Thermohaline forcing of eastern boundary currents: With application to the circulation off the west coast of Australia. *J. Mar. Res.*, **44**, 71–92, https://doi.org/10.1357/002224086788460184.

Meincke, J., G. Siedler, and W. Zenk, 1975: Some current observations near the continental slope off Portugal. *Meteor-Forschungsergeb. Reihe A*, **16**, 15–22.

Mittelstaedt, E., 1976: On the currents along the Northwest African coast South of 22° North. *Dtsch. Hydrogr. Z.*, **29**, 97–117, https://doi.org/10.1007/BF02227058.

——, 1983: The upwelling area off Northwest Africa—A description of phenomena related to coastal upwelling. *Prog. Oceanogr.*, **12**, 307–331, https://doi.org/10.1016/0079-6611(83)90012-5.

——, 1989: The subsurface circulation along the Moroccan slope. *Poleward Flows along Eastern Ocean Boundaries*, S. J. Neshyba et al., Eds., Coastal and Estuarine Studies, Vol. 34, Amer. Geophys. Union, 96–109.

——, D. Pillsbury, and R. L. Smith, 1975: Flow patterns in the Northwest African upwelling area. *Dtsch. Hydrogr. Z.*, **28**, 145–167, https://doi.org/10.1007/BF02232617.

Nelson, G., 1989: Poleward motion in the Benguela area. *Poleward Flows along Eastern Ocean Boundaries*, S. J. Neshyba et al., Eds., Coastal and Estuarine Studies, Vol. 34, Amer. Geophys. Union, 110–130.

Neshyba, S. J., C. N. K. Mooers, R. L. Smith, and R. T. Barber, 1989: Poleward flows along eastern ocean boundaries: An introduction and historical review. *Poleward Flows along Eastern Ocean Boundaries*, S. J. Neshyba et al., Eds., Coastal and Estuarine Studies, Vol. 34, Amer. Geophys. Union, 17–25.

Ollitrault, M., and A. Colin de Verdière, 2013: The Ocean General Circulation near 1000-m depth. *J. Phys. Oceanogr.*, **44**, 384–409, https://doi.org/10.1175/JPO-D-13-030.1.

Pawlowicz, R., 2020: M_Map: A mapping package for MATLAB, version 1.4m. www.eoas.ubc.ca/~rich/map.html.

Pelegrí, J. L., J. Arístegui, A. Hernández-Guerra, S. Hernández-León, A. Marrero-Díaz, M. F. Montero, and P. Sangrà, 2005: Coupling between the open ocean and the coastal upwelling region off northwest Africa: Water recirculation and offshore pumping of organic matter. *J. Mar. Syst.*, **54**, 3–37, https://doi.org/10.1016/j.jmarsys.2004.07.003.

Peliz, Á., J. Dubert, D. Haidvogel, and B. Le Cann, 2003: Generation and unstable evolution of a density-driven eastern poleward current: The Iberian Poleward Current. *J. Geophys. Res.*, **108**, 3268, https://doi.org/10.1029/2002JC001443.

——, ——, A. M. P. Santos, P. B. Oliveira, and B. Le Cann, 2005: Winter upper ocean circulation in the Western Iberian Basin—Fronts, eddies and poleward flows: An overview. *Deep-Sea Res. I*, **52**, 621–646, https://doi.org/10.1016/j.dsr.2004.11.005.

Peña-Izquierdo, J., J. L. Pelegrí, M. V. Pastor, P. Castellanos, M. Emelianov, M. Gasser, J. Salvador, and E. Vázquez-Domínguez, 2012: The continental slope current system between Cape Verde and the Canary Islands. *Sci. Mar.*, **76**, 65–78, https://doi.org/10.3989/scimar.03607.18C.

Pérez-Hernández, M. D., A. Hernández-Guerra, E. Fraile-Nuez, I. Comas-Rodríguez, V. M. Benítez-Barrios, J. F. Domínguez-Yanes, P. Vélez-Belchí, and D. De Armas, 2013: The source of the Canary current in fall 2009. *J. Geophys. Res. Oceans*, **118**, 2874–2891, https://doi.org/10.1002/jgrc.20227.

——, G. D. McCarthy, P. Vélez-Belchí, D. A. Smeed, E. Fraile-Nuez, and A. Hernández-Guerra, 2015: The Canary Basin contribution to the seasonal cycle of the Atlantic Meridional Overturning Circulation at 26°N. *J. Geophys. Res. Oceans*, **120**, 7237–7252, https://doi.org/10.1002/2015JC010969.

Prieto, E., C. González-Pola, A. Lavín, R. F. Sánchez, and M. Ruiz-Villarreal, 2013: Seasonality of intermediate waters hydrography west of the Iberian Peninsula from an 8 year semiannual time series of an oceanographic section. *Ocean Sci.*, **9**, 411–429, https://doi.org/10.5194/os-9-411-2013.

Risien, C. M., and D. B. Chelton, 2008: A global climatology of surface wind and wind stress fields from eight years of QuikSCAT scatterometer data. *J. Phys. Oceanogr.*, **38**, 2379–2413, https://doi.org/10.1175/2008JPO3881.1.

Roemmich, D., and J. Gilson, 2009: The 2004–2008 mean and annual cycle of temperature, salinity, and steric height in the global ocean from the Argo Program. *Prog. Oceanogr.*, **82**, 81–100, https://doi.org/10.1016/j.pocean.2009.03.004.

Sangrà, P., C. Troupin, B. Barreiro-González, E. Desmond Barton, A. Orbi, and J. Arístegui, 2015: The Cape Ghir filament system in August 2009 (NW Africa). *J. Geophys. Res. Oceans*, **120**, 4516–4533, https://doi.org/10.1002/2014JC010514.

Shillington, F. A., C. J. C. Reason, C. M. Duncombe Rae, P. Florenchie, and P. Penven, 2006: Large scale physical variability of the Benguela Current Large Marine Ecosystem (BCLME). *Benguela: Predicting a Large Marine Ecosystem*, V. Shannon et al. Eds., Large Marine Ecosystems, Vol. 14, Elsevier, 49–70, https://doi.org/10.1016/S1570-0461(06)80009-1.

Teles-Machado, A., Á. Peliz, J. C. McWilliams, X. Couvelard, and I. Ambar, 2016: Circulation on the Northwestern Iberian Margin: Vertical structure and seasonality of the alongshore flows. *Prog. Oceanogr.*, **140**, 134–153, https://doi.org/10.1016/j.pocean.2015.05.021.

Thomson, R. E., and M. V. Krassovski, 2010: Poleward reach of the California Undercurrent extension. *J. Geophys. Res.*, **115**, C09027, https://doi.org/10.1029/2010JC006280.

Thyng, K. M., C. A. Greene, R. D. Hetland, H. M. Zimmerle, and S. F. DiMarco, 2016: True colors of oceanography: Guidelines for effective and accurate colormap selection. *Oceanography*, **29**, 9–13, https://doi.org/10.5670/oceanog.2016.66.

Todd, R. E., D. L. Rudnick, M. R. Mazloff, R. E. Davis, and B. D. Cornuelle, 2011: Poleward flows in the southern California Current System: Glider observations and numerical simulation. *J. Geophys. Res.*, **116**, C02026, https://doi.org/10.1029/2010JC006536.

Vélez-Belchí, P., M. D. Pérez-Hernández, M. Casanova-Masjoan, L. Cana, and A. Hernández-Guerra, 2017: On the seasonal variability of the Canary Current and the Atlantic Meridional Overturning Circulation. *J. Geophys. Res. Oceans*, **122**, 4518–4538, https://doi.org/10.1002/2017JC012774.

Wang, D.-P., 1982: Effects of continental slope on the mean shelf circulation. *J. Phys. Oceanogr.*, **12**, 1524–1526, https://doi.org/10.1175/1520-0485(1982)012<1524:EOCSOT>2.0.CO;2.

Zenk, W., and L. Armi, 1990: The complex spreading pattern of Mediterranean Water off the Portuguese continental slope. *Deep-Sea Res.*, **37A**, 1805–1823, https://doi.org/10.1016/0198-0149(90)90079-B.